Optimality

www.opt.reapress.com

Opt. Vol. 1, No. 2 (2024) 287–299.

Paper Type: Original Article

MHD Flow and Heat Transfer of a Hybrid Nanofluid Past a Permeable Stretching/Shrinking Wedge

Prasanta Parida[1], Kharabela Swain[2,*], Hibah Islahi[1]

[1] Institute of Applied Sciences, Mangalayatan University, Aligarh-202146, India; prasantaparidapkp.333@gmail.com; hibah.islahi@mangalayatan.edu.in.

[2] Department of Mathematics, GIFT Autonomous College, Bhubaneswar-752054, India; kharabela1983@gmail.com.

Citation:

Received: 4 June 2024 *Revised: 19 August 2024* *Accepted: 27 September 2024*	Parida, P., Swain, Kh., & Islahi, H. (2024). MHD flow and heat transfer of a hybrid nanofluid past a permeable stretching/shrinking wedge. *Optimality*, *1*(2), 287-299.

Abstract

The present article intends to discuss the flow of an electromagnetic hybrid nanofluid over an expanding/contracting wedge considering the combination of the oxide particle alumina and the metal particle copper in conventional fluid water. Further, the heat transport phenomenon is enhanced for the inclusion of thermal radiation. Following the recent applications used in industrial production processes, cooling of electronic devices, peristaltic pumping processes, drug delivery systems, blood flow through arteries, etc., the role of nanofluid, as well as hybrid nanofluid, is important. The proposed assumptions govern the flow phenomenon are nonlinear and partial. Therefore, appropriate similarity transformation is used for the conversion of non-dimensional ordinary equations and further, traditional numerical technique is adopted to handle the governing equations. The physical properties of the parameters involved are simulated through graphs and tables.

Keywords: Hybrid nanofluid, Stretching/shrinking wedge, Magnetic field, Radiation, Numerical technique.

1 | Introduction

An advanced type of nanofluid is called a hybrid nanofluid, which has two different nanoparticles dispersed in the primary fluid. Initially, Choi and Eastman [1] studied the nanofluid to enhance the base fluid's thermal conductivity in addition to nanoparticles. Due to its capacity to increase the heat transfer rate compared to base fluid and nanofluid, the heat transfer of hybrid nanofluid has gained much attention from researchers in recent years. Due to this, hybrid nanofluid has been considered the heat transfer fluid in most heat transfer applications, including coolant in machining, electronic cooling, and transformer cooling. In particular, hybrid nanofluid is well known as a fluid with a higher heat transmission rate than standard regular fluid. Devi and

Corresponding Author: kharabela1983@gmail.com

https://doi.org/10.22105/opt.v1i2.33

Devi [2] examined the hybrid nanofluid flow past a stretching surface, considering copper and alumina as nanoparticles.

The flow past a wedge-shaped surface with heat transfer has gained extensive attention in recent decades. It is attributed to its numerous applications in the chemical industry and engineering, such as aerodynamics and geothermal industries. Historically, this type of flow was first proposed by Falkner and Skan [3] to show the application of Prandtl's theory of boundary layers. The ordinary (similarity) differential equations were obtained using similarity transformation techniques. Nowadays, these equations are currently known as the Falkner-Skan equation. Later, Hartee [4] introduced the Hartee pressure gradient parameter into the Falkner-Skan equation and then solved the equation numerically. Riley and Weidman [5] demonstrated the Falkner-Skan flow over a stretching surface and obtained multiple solutions. After that, the works on Falkner-Skan flow were conducted by many researchers.

Furthermore, the problem of stretching/shrinking wedge was explored by Alam et al. [6], considering the variable fluid properties and thermophoresis effects with variable Schmidt and Prandtl numbers. Later, Khan et al. [7] studied the nanofluid flow past a nonlinearly stretching or shrinking wedge with the Brownian motion, magnetic field, nonlinear radiation and thermophoresis effects. Awaludin et al. [8] examined the viscous flow problem with magnetic field effects over a stretching/shrinking wedge. The dual solutions were obtained for the shrinking wedge, whereas the solution is unique for the stretching wedge case. Waini et al. [9] considered hybrid nanofluid flow towards a stagnation point region with second-order slip.

Further, Waini et al. [10] studied hybrid nanofluid flow and heat transfer past a permeable stretching/shrinking surface with a convective boundary condition. Swain et al. [11] studied the effects of MWCNT and Fe3O4 nanoparticles on an exponentially porous shrinking sheet with chemical reactions and slip boundary conditions. Dinarvand et al. [12] examined the unsteady flow of a hybrid nanofluid past a stretching sheet. Lund et al. [13] examined the stability analysis of a hybrid nanofluid over a stretching sheet. Thumma and Mishra [14] investigated the effects of dissipation and Joule heating on the MHD Jeffery nanofluid flow. The movement of a micropolar nanofluid over a stretched sheet was taken into account by Pattnaik et al. [15]. Thumma et al. [16] recently investigated how cupric oxide and silver nanoparticles affected the flow of a nanofluid when the Coriolis force was present. Khashi'ie et al. [17] studied the MHD flow of a hybrid nanofluid over a moving plate with Joule heating. Lund et al. [18] considered the stability analysis of magnetized hybrid nanofluid propagating through an unsteady shrinking sheet. Many authors have studied the hybrid nanofluid flow using different flow models [19]–[28].

Motivated by the above-mentioned studies, in the present paper, we investigate the flow of an electromagnetic hybrid nanofluid over an expanding/contracting wedge considering the combination of the oxide particle alumina and the metal particle copper in the conventional fluid water. Further, the heat transport phenomenon is enhanced by including thermal radiation. Using similarity transformation, the leading partial differential equations are converted into non-linear ordinary differential equations which are solved numerically by MATLAB software using bvp4c code. Graphs and tables depict different characterising factors' consequences on the flow model.

2 | Mathematical Formulation

Consider a steady hybrid nanofluid flow and heat transfer past a permeable stretching/shrinking wedge as displayed in *Fig. 1*, where x and y are Cartesian coordinates with $x-$axis measured along the surface of the wedge and the $y-$axis normal to it. The free stream velocity is $u_e(x)=U_e x^m$ while the wedge is stretched/shrunk with a velocity $u_w(x)=U_w x^m$, where U_e is a positive constant, while U_w is a positive constant corresponding to the stretching wedge, U_w is a negative constant corresponding to the shrinking wedge and $U_w=0$ for a static wedge. Here, $m=\frac{\beta}{(2-\beta)}$ where m and β represent the angle of the wedge and the Hartree pressure gradient parameters, respectively, while $\Omega=\beta\pi$ is the total angle of the wedge. Further, we note that the value of m is between 0 and 1, with $m = 0(\beta = 0)$ representing the flow past a horizontal flat surface $(\Omega = 0)$, and $m = 1(\beta = 1)$ represents the stagnation point flow toward a vertical surface $(\Omega = \pi)$. In this study, we consider the wedge flow problem, so that the value of m must be in the range of $0 < m < 1$. In addition, the value of m is taken from $0.1 < m < 0.3$ to represent the acute wedge angle, where the wedge angle Ω is between 0 and $\pi/2$. The hybrid nanofluid has constant ambient temperature T_∞, where the constant temperature of the stretching/shrinking wedge is T_w. A magnetic field $B(x)$ is applied in the $y-$direction with $B(x) = B_0 x^{(m-1)/2}$, where B_0 is the applied magnetic field strength. The magnetic Reynolds number is assumed to be small so that the induced magnetic field is neglected.

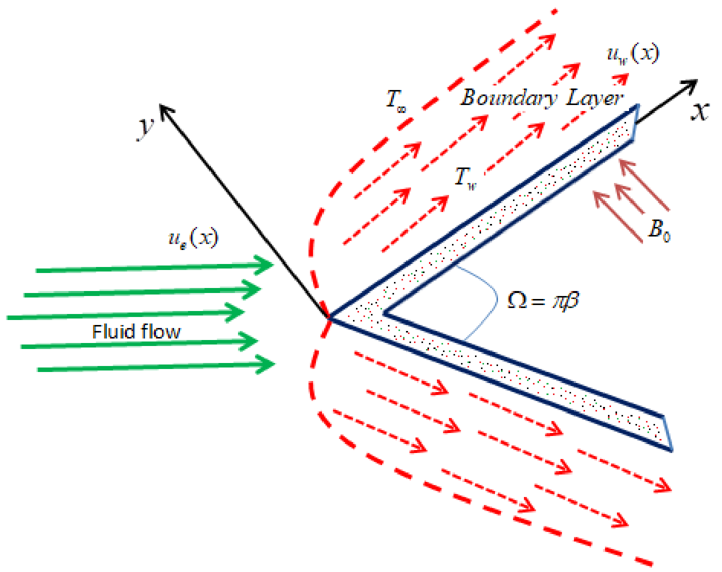

Fig. 1. Physical model and coordinate system for stretching wedge, and shrinking wedge.

After applying the boundary layer approximations as well as Bernoulli's equation in the free stream, the governing equations of the hybrid nanofluid can be written as follows:

$$\frac{\partial u}{\partial x} + \frac{\partial u}{\partial y} = 0, \tag{1}$$

$$u\frac{\partial u}{\partial x} + v\frac{\partial u}{\partial y} = u_e \frac{du_e}{dx} + \frac{\mu_{hnf}}{\rho_{hnf}}\frac{\partial^2 u}{\partial y^2} - \frac{\sigma_{hnf}}{\rho_{hnf}} B^2 (u - u_e), \tag{2}$$

$$u\frac{\partial T}{\partial x} + v\frac{\partial T}{\partial y} = \frac{k_{hnf}}{(\rho C_p)_{hnf}}\frac{\partial^2 T}{\partial y^2} - \frac{1}{(\rho C_p)_{hnf}}\frac{\partial q_r}{\partial y}. \tag{3}$$

The prescribed boundary conditions are

$$\left.\begin{array}{l} v = v_w(x), u = v_w(x), T = T_w, \\ u \to u_e(x), T \to T_\infty, \text{as}, y \to \infty \end{array}\right\}, \tag{4}$$

where u and v represent the velocity components of the hybrid nanofluid along the $x-$axes and $y-$ axes, respectively, T denotes the hybrid nanofluid temperature, q_r indicates the radiative heat flux, and $v_w(x)$ represents the velocity of the wall mass transfer. According to the Rosseland approximation, the radiative heat flux is simply expressed as follows:

$$q_r = -\frac{4\sigma_0}{3k^*}\frac{\partial T^4}{\partial y}, \tag{5}$$

where k^* and σ_0 denote the mean absorption coefficient and the Stefan-Boltzmann constant, respectively. Using the Taylor series and ignoring the higher order terms, T^4 is expanded about T_∞ to obtain $T^4 \approx 4T_\infty^3 T - 3T_\infty^4$. Then, *Eq. (3)* can be written as

$$u\frac{\partial T}{\partial x}+v\frac{\partial T}{\partial y}=\left(\frac{k_{hnf}}{(\rho C_p)_{hnf}}+\frac{16\sigma_0 T_\infty^3}{3k^*(\rho C_p)_{hnf}}\right)\frac{\partial^2 T}{\partial y^2}. \quad (6)$$

Further, $\mu_{hnf}, \sigma_{hnf}, \rho_{hnf}, k_{hnf}$ and $(\rho C_p)_{hnf}$ are the dynamic viscosity, electrical conductivity, density, thermal conductivity and heat capacity of the hybrid nanofluid, respectively. Following Gherasim et al. [29] and Mintsa et al. [30], *Table 1* provides the thermo physical properties of nanofluid and hybrid nanofluid. In *Table 1*, φ_1 and φ_2 are the volume fractions of Cu and Al_2O_3 nanoparticles, respectively, where $\varphi_1 = \varphi_2 = 0$ represent the regular fluid, μ represents the dynamic viscosity, ρ is the density, C_p is the specific heat at constant pressure, $(\rho C_p)_{hnf}$ is the heat capacity, k is the thermal conductivity and σ is the electrical conductivity in which the subscripts $hnf, nf, f, s1$ and $s2$ represent hybrid nanofluid, nanofluid, fluid, and solid components for Al_2O_3 and Cu nanoparticles, respectively. *Table 2* provides the physical properties of water, Cu and Al_2O_3 nanoparticles [31].

Following Waini et al. [21], we apply the following similarity variables:

$$\psi=\left(U_e\upsilon_f\right)^{1/2}x^{(m+1)/2}f(\eta),\theta(\eta)=\frac{T-T_\infty}{T_w-T_\infty},\eta=\left(\frac{U_e}{\upsilon_f}\right)^{1/2}x^{(m-1)/2}y, \quad (7)$$

where ψ is the stream function defined by $u=\frac{\partial\psi}{\partial y}$ and $v=\frac{\partial\psi}{\partial x}$ which satisfies *Eq. (1)* and υ_f is the base fluid kinematic viscosity. Thus, the velocities are expressed as

$$u=U_e x^m f'(\eta), v=\frac{m+1}{2}\left(U_e\upsilon_f\right)^{1/2}x^{(m-1)/2}\left(f(\eta)+\frac{m-1}{m+1}\eta f'(\eta)\right), \quad (8)$$

To obtain similarity, we take

$$v_w(x)=\frac{m+1}{2}\left(U_e\upsilon_f\right)^{1/2}x^{(m-1)/2}S, \quad (9)$$

where $S=f(0)$ is the parameter of constant mass flux with $S>0$ represents fluid suction, while $S<0$ representing fluid injection or removal.

Using *Eq. (7)* into *Eqs. (2)* and *(6)*, we get the similarity equations as follows:

$$\frac{\mu_{hnf}/\mu_f}{\rho_{hnf}/\rho_f}f'''+\frac{m+1}{2}ff''+m\left(1-f'^2\right)-\frac{\sigma_{hnf}/\sigma_f}{\rho_{hnf}/\rho_f}M\left(f'-1\right)=0, \quad (10)$$

$$\frac{1}{(\rho Cp)_{hnf}/(\rho Cp)_f}\left(\frac{k_{hnf}}{k_f}+\frac{4}{3}R\right)\theta''+\frac{m+1}{2}\Pr f\theta'=0, \quad (11)$$

and the boundary conditions *Eq. (4)* become

$$\left.\begin{array}{l} f(0)=S, f'(0)=\lambda, \theta(0)=1, \\ f'(\eta)\to 1, \theta(\eta)\to 0, \text{as}, \eta\to\infty \end{array}\right\}, \quad (12)$$

where the Prandtl $(\Pr)$ number, the magnetic parameter M, the radiation parameter R, and the stretching/shrinking parameter λ are defined as $\Pr=\frac{\upsilon_f}{\alpha_f}, M=\frac{\sigma_f B_0^2}{\rho_f U_e}, R=\frac{4\sigma_0 T_\infty^3}{k_1 k^*}, \lambda=\frac{U_w}{U_e}$.

Here, $\lambda > 0$ for stretching, $\lambda < 0$ for shrinking, and $\lambda = 0$ for a static wedge. It is worth mentioning that by considering regular fluid $(\varphi_1 = \varphi_2 = 0)$ with no magnetic field effects for $m = 0$, *Eq. (10)* reduces to that of the classical Blasius problem as discussed by Blasius for the case when $S = 0$ and $\lambda = 0$.

The physical quantities of interest are the skin friction coefficient C_f and local Nusselt number Nu_x are defined as $C_f = \frac{T_w}{\rho_f u_e^2}, Nu_x = \frac{x q_w}{k_f (T_w - T_\infty)}$, respectively.

Here T_w denotes the surface shear stress over the wedge, and q_w denotes the heat flux from the wedge surface, which are respectively given by

$$T_w = \mu_{hnf}\left(\frac{\partial u}{\partial y}\right)_{y=0}, q_w = -k_{hnf}\left(\frac{\partial T}{\partial y}\right)_{y=0} + (q_r)_y = 0.$$

Finally, we get $Re_x^{1/2} C_f = \frac{\mu_{hnf}}{\mu_f} f''(0), Re_x^{-1/2} Nu_x = -\left(\frac{k_{hnf}}{k_f} + \frac{4}{3}R\right)\theta'(0)$, where $Re_x = U_e(x)x/\upsilon_f$ is the local Reynolds number.

Table 1. Thermophysical properties of nanofluid and hybrid nanofluid [29], [30].

Properties	Nanofluid	Hybrid Nanofluid
Density	$\rho_{nf} = (1-\varphi_1)\rho_f + \varphi_1\rho_{n1}$	$\rho_{hnf} = (1-\varphi_2)\rho_{nf} + \varphi_2\rho_{n2}$
Dynamic viscosity	$\mu_{nf} = \mu_f (0.904)e^{14.8\varphi_1}$	$\mu_{hnf} = \mu_{nf} (0.904)e^{14.8\varphi_2}$
Thermal conductivity	$k_{nf} = k_f (1+1.72\varphi_1)$	$k_{hnf} = k_{nf} (1+1.72\varphi_2)$
Heat capacity	$(\rho C_p)_{nf} = (1-\varphi_1)(\rho C_p)_f + \varphi_1(\rho C_p)_{n1}$	$(\rho C_p)_{hnf} = (1-\varphi_2)(\rho C_p)_{nf} + \varphi_2(\rho C_p)_{n2}$
Electrical conductivity	$\frac{\sigma_{nf}}{\sigma_f} = 1 + \frac{3\left(\frac{\sigma_{n1}}{\sigma_f} - 1\right)\varphi_1}{\frac{\sigma_{n1}}{\sigma_f} + 2 - \left(\frac{\sigma_{n1}}{\sigma_f} - 1\right)\varphi_1}$	$\frac{\sigma_{hnf}}{\sigma_{nf}} = 1 + \frac{3\left(\frac{\sigma_{n2}}{\sigma_{nf}} - 1\right)\varphi_2}{\frac{\sigma_{n2}}{\sigma_{nf}} + 2 - \left(\frac{\sigma_{n2}}{\sigma_{nf}} - 1\right)\varphi_2}$

Table 2. Thermo-physical properties of water and nanoparticles [31].

Properties	$\rho(kg/m^3)$	$C_p(J/kgK)$	$k(W/mK)$	$\sigma(s/m)$
Water	997.1	4179	0.613	5.5×10^{-6}
Cu	8933	385	400	5.96×10^{7}
Al_2O_3	3970	765	40	3.69×10^{7}

Table 3. Comparison of $f''(0)$ for different values of λ when M=R=S=$\phi_1 = \phi_2$=0 and m=1.

λ	$f''(0)$		
	Wang [32]	Bachok et al. [33]	Present Study
2.0	-1.88731	-1.887307	-1.889263
1.0	0	0	0
0.5	0.71330	0.713295	0.716018
0	1.232588	1.232588	1.241326
-0.5	1.49567	1.495670	1.520170
-1.0	1.32882	1.328817	1.420621

3 | Results and Discussion

The two-dimensional flow of hybrid nanofluid is discussed due to the inclusion of the magnetic parameter in the current investigation. The magnetized fluid, in association with the various nanoparticles composed of alumina (Al_2O_3) and metal particle Copper (Cu) in the base liquid water, performs their characteristic. The conjunction of thermal radiation for the assumption of Rosseland's approximation enriches the flow profile significantly. *Table 1* indicates the physical phenomena of the thermal properties such as viscosity, thermal conductivity, electrical conductivity, density, etc., for the nanofluid as well as hybrid nanofluid following the empirical work of Gherasim et al. [29] and Mintsa et al. [30]. Further, the numerical values of these quantities for a normal temperature of 298^0K are presented in *Table 2*. The benchmark result for the comparative study with the earlier work of Wang [32] and Bachok et al. [33] shows a good correlation to that of the current result of shear rate in the particular case, and that is presented in *Table 3*. However, *Table 4* shows the rate of heat transfer for the case of nanofluid and the simulated results are compared with the work of Yacob et al. [34] and the Bachok et al. [33]. These simulations also show a good correlation with the current study. It validates the current results as well as confirms the convergence criteria of the methodology adopted. Further, throughout the computation, we fixed the values of the non-dimensional parameters as $M = 0.5, m = 2, R = 0.3, S = L = 0.5, \phi_1 = \phi_2 = 0.02, Pr = 6.2$ except those where the particular variation is deployed in the corresponding figure. The special cases of the governing equations are obtained for the various values of the power-law index parameter as described in the earlier section that validates with the work of Blasius and Sparrow as compared to *Eqs. (10)* and *(11)*. The behaviour of the significant parameters imposed in the flow phenomena is presented through *Figs. 2-9* and elaborated briefly.

Fig. 2 illustrates the consequences of the power-law index (m) for the various values of the magnetic parameter (M) on the fluid velocity distribution. The non-zero values of the particle concentration (ϕ_1, ϕ_2) suggest the behaviour is established for the hybrid nanofluid due to the occurrence of the other characterising constraints displayed in the figure. The higher values of M are considered in dottedlines whereas the lower values of M treated as bold lines. The comparative results shows for the non-occurrence of the index parameter, i.e., $m = 0$ leads to the particular case of classical Blasius flow and behaviour shows that for $m = 0$ the fluid exhibits the lower velocity profile throughout the domain.

However, increasing index parameter enhances the velocity in magnitude but really in this case the bounding surface thickness retards. This fact is exhibited due to the involvement of the resistive force i.e. the magnetic parameter. Further, higher magnetization also explores the lower in thickness in comparison to the lower magnetization. The fact is because of the involvement of the resistive force has a significant property to produce Lorentz force that has the tendency to decelerates the thickness. *Fig. 3* contributes the role of the suction for the variation of the velocity ratio parameter. Dual nature in the profile is exhibited for the variation of ratio parameter (λ). In particular for $(L = 1)$ the profile behaves linearly, whereas $(L > 1)$ moves in upward shows in dotted and for $L < 1$ the direction of the profile downward presented in bold lines. The suction pressure exhibits its significant behaviour within the flow domain. It is seen that increasing suction decelerates in the upper half, and the in the lower half, the increasing suction overshoots the profile throughout the domain. In both of the cases the effect of suction deliberates its greater retardation in the bounding surface thickness.

Fig. 4 characterizes the significant role of the nanoparticle concentration on the fluid velocity. The flow profile is encouraged due to the inclusion of the particle concentration and their physical properties described earlier. Here, the various conditions, such as the case of pure fluid, i.e., $\phi_1 = 0 = \phi_2$, the case of nanofluid, i.e., $\phi_1 = 0, \phi_2 \neq 0$, and the case of hybrid nanofluid, i.e., $\phi_1 \neq 0, \phi_2 = 0$ are discussed. The present figure shows that the case of pure fluid exhibits maximum velocity near the surface region however, the inclusion of particle concentration of both Cu and Al_2O_3 retards it significantly resulting the thickness of the bounding surface enhanced. Therefore, the recent advancement in the applications used in the production processes hybrid nanofluid is used to control over the shape of the product avoiding the maximum damage.

The fluid temperature is characterized by the thermophysical properties of conductivity and specific heat organized by the particle concentration is displayed in *Fig. 5*. The variation of the particle concentration is presented for the varied values of suction $(S=1)$ /injection $(S=-1)$ (flow through permeable surface) as well as the flow through impermeable surface $(S=0)$. The analysis is exhibited by the three layer variation presented in the corresponding figure. The increasing particle concentration overshoots the fluid temperature for $S=1$ and $S=0$ whereas the case of injection decelerates it but the resulting behaviour is insignificant. *Fig. 6* portrays the role of the power-law index on the fluid temperature distribution for the various values of the radiation parameter. Thermal radiation is the transformation of electromagnetic radiation emitted from the fluid particle within the medium. The amount of emitted particle is organized by the radiation parameter. The increasing power-law index retards the temperature profile and in comparison to the classical Blasius flow it is seen that the fluid temperature shows its maximum strength within the entire domain. The behaviour of the profile seems to be asymptotic to meet the requisite boundary conditions. Further, enhanced thermal radiation overshoots the profile so that the fluid temperature augments. *Fig. 7* exhibits the behaviour of the velocity ratio on the fluid temperature due to the involvement of the case of nanofluid and hybrid nanofluid. The observation reveals that increasing the velocity ratio attenuates the fluid temperature exhibiting a controlling parameter.

Finally, the numerical computation of the shear rate coefficient for the various characterizing parameters is presented in *Table 5*. The result shows that increasing concentration enhances the shear rate coefficients in the case of suction, and $L=0.5$ further, $L=1.5$ the values of shear rate also increase in magnitude. A similar observation is rendered for the case of injection.

Table 6 explored the variation of the particle concentration and the radiation effect on the heat transfer rate with the variation of magnetic parameters. Dual characteristic is observed in the case of nanofluid and the case of hybrid nanofluid. In the case of nanofluid, increasing particle concentration enhances the rate, whereas the case of hybrid nanofluid retards the coefficient significantly. Increasing magnetic parameter retards the heat transfer rate significantly. *Table 7* renders the effect of various parameters like the power-law index, suction, velocity ratio parameter and the Prandtl number on the heat transfer rate. The rate decreases for increasing all these parameters.

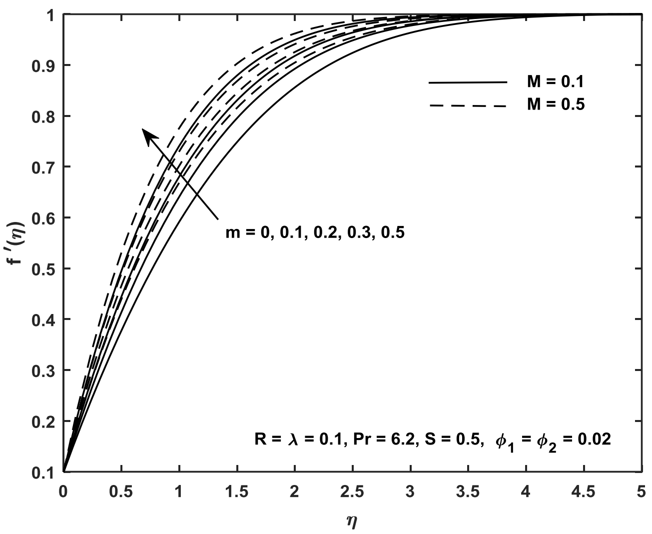

Fig. 2. Velocity profile versus m and M.

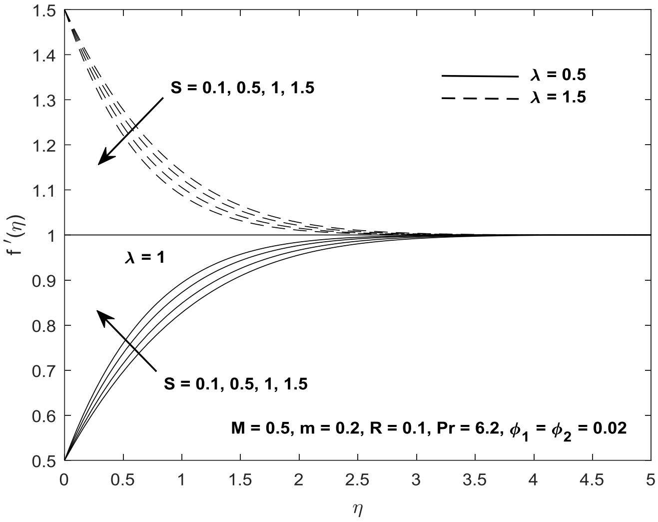

Fig. 3. Velocity profile versus **S** and **λ**.

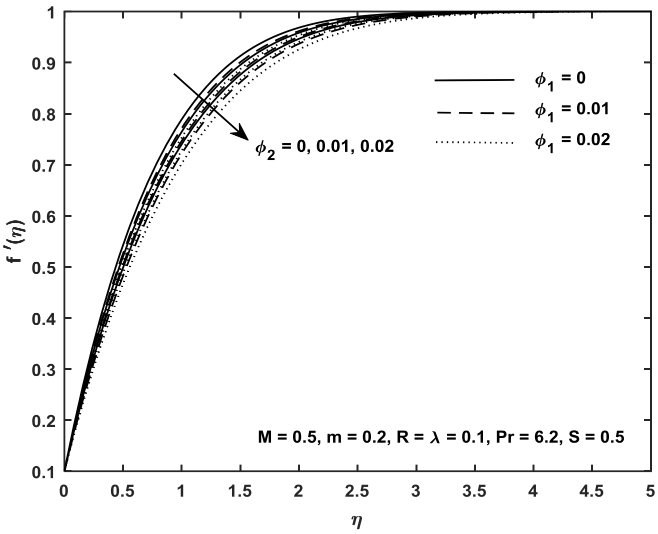

Fig. 4. Velocity profile versus ϕ_1 and ϕ_2.

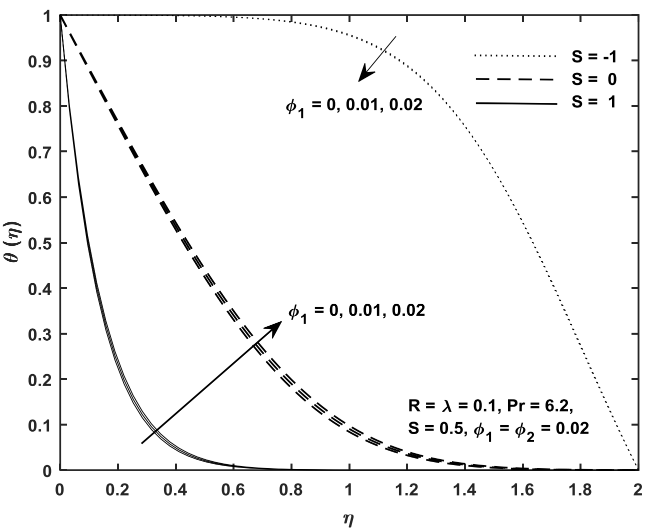

Fig. 5. Temperature profile versus **S** and ϕ_1.

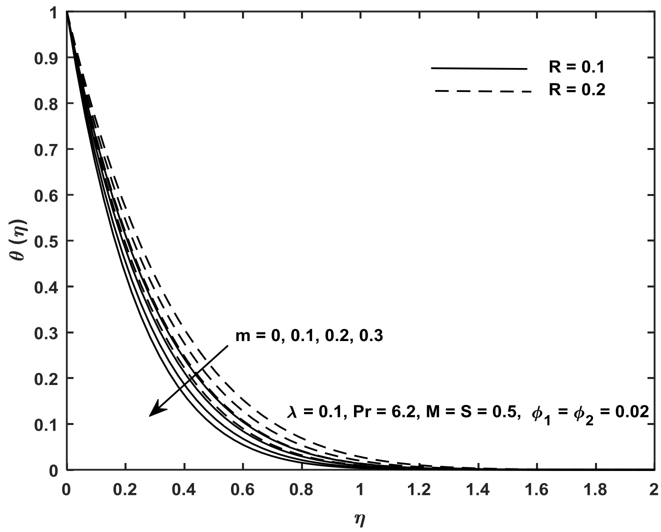

Fig. 6. Temperature profile versus m and R.

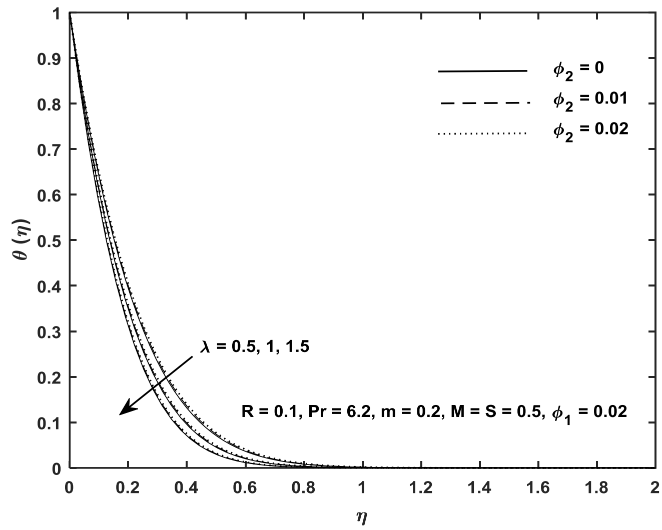

Fig. 7. Temperature profile versus λ and ϕ_2.

Table 4. Comparison of $-\theta'(0)$ for different values of λ and ϕ_1 when M=R=S=ϕ_2=0 and m=1.

λ	ϕ_1	$-\theta'(0)$					
		Yacob et al. [34]		Bachok et al. [33]		Present Study	
		Cu-Water	Al_2O_3-Water	Cu-Water	Al_2O_3-Water	Cu-Water	Al_2O_3-Water
-0.5	0.1			0.8385	0.7272	0.85105	0.75461
	0.2			1.0802	0.8878	1.10402	0.94326
0	0.1	1.4043	1.3305	1.4043	1.3305	1.40686	1.33655
	0.2	1.6692	1.5352	1.6692	1.5352	1.67574	1.54972
0.5	0.1			1.8724	1.8278	1.87291	1.82911
	0.2			2.1577	2.0700	2.15956	2.07360

Table 5. Computational values of $Re_x^{1/2}C_f$ for various values of S, ϕ_1, ϕ_2 and L when $M = 0.5, R = 0.1, Pr = 6.2$.

S	ϕ_1	ϕ_2	L	$f''(0)$
0.5	0	0	0.5	0.559365
	0.01	0		0.618665
	0.02	0		0.683524
	0.02	0.01		0.743505
	0.02	0.02		0.810426
	0	0	1.5	-0.628582
	0.01	0		-0.696248
	0.02	0		-0.769994
	0.02	0.01		-0.836269
	0.02	0.02		-0.909606
-0.5	0	0	0.5	0.395421
	0.01	0		0.441840
	0.02	0		0.493951
	0.02	0.01		0.550165
	0.02	0.02		0.613408
	0	0	1.5	-0.463778
	0.01	0		-0.518435
	0.02	0		-0.579282
	0.02	0.01		-0.641594
	0.02	0.02		-0.711071

Table 6. Computational values of $-\theta'(0)$ for various values of M, ϕ_1, ϕ_2 and R when $m = 2, S = \lambda = 0.5$ and $Pr = 6.2$.

M	ϕ_1	ϕ_2	R	$-\theta'(0)$
0.1	0	0	0.1	5.151905
	0.01	0		5.153484
	0.02	0		5.154972
	0.02	0.01		5.144734
	0.02	0.02		5.134553
	0	0	0.3	5.393105
	0.01	0		5.392359
	0.02	0		5.391442
	0.02	0.01		5.378288
	0.02	0.02		5.365275
1.0	0	0	0.1	5.156049
	0.01	0		5.157515
	0.02	0		5.158903
	0.02	0.01		5.148639
	0.02	0.02		5.138423
	0	0	0.3	5.399719
	0.01	0		5.398741
	0.02	0		5.397621
	0.02	0.01		5.384434
	0.02	0.02		5.371371

Table 7. Computational values of $-\theta'(0)$ for various values of m, S, λ and Pr when $M = 0.5, \phi_1 = \phi_1 = 0.02$ and $R = 0.3$

m	S	λ	Pr	$-\theta'(0)$
0.1	0.1	0.1	6.2	1.001674
1.0				1.484213
2.0				1.952675
	0.2			2.642462
	0.3			3.395900
		0.5		3.785631
		1.0		4.200895
		1.5		4.562363
			7	4.998370
			10	6.575941
			12	7.592992

4 | Conclusion

Numerical treatment is adopted for the flow of hybrid nanofluid past a horizontal wedge for the impact of particle concentration due to the occurrence of the magnetic parameter, and the thermal radiation is presented briefly. The behaviour of the concentration affecting the flow as well as temperature distributions are presented and deliberated for the required quantities of the contributing parameters within their range. Further, the major outcomes are presented below:

I. The validation and the comparative study of the present simulated result with the earlier investigation show the conformity as well as the convergence criteria of the current methodology and also provide the right direction to carry out the study.

II. The role of the power-law index signifies the comparison between the classical governing equation and, further, the enhanced values of the index parameter provide greater retardation in the thickness of the velocity and the thermal bounding surface thickness.

III. A dual characteristic is observed in the velocity distribution for the variation of suction pressure due to the occurrence of the different velocity ratios. An interesting feature is exhibited, showing the linear relation if the ratio is unity.

IV. Particle concentration decelerates the fluid velocity and enhances the fluid temperature profile irrespective of the case of nanofluid and the hybrid nanofluid that overrides the fact of the pure fluid.

V. Enhanced concentration augments the shear rate in magnitude irrespective of the values of the velocity ratio and the rate of heat transfer enhances for the increasing values of the contributing parameters.

Conflict of Interest

The authors declare no conflict of interest.

Data Availability

All data are included in the text.

Funding

This research received no specific grant from funding agencies in the public, commercial, or not-for-profit sectors.

References

[1] Choi, S. U. S., & Eastman, J. A. (1995). *Enhancing thermal conductivity of fluids with nanoparticles*. https://www.osti.gov/biblio/196525

[2] Devi, S. P. A., & Devi, S. S. U. (2016). Numerical investigation of hydromagnetic hybrid Cu--Al2O3/water nanofluid flow over a permeable stretching sheet with suction. *International journal of nonlinear sciences and numerical simulation*, *17*(5), 249–257. https://doi.org/10.1515/ijnsns-2016-0037

[3] Falkneb, V. M., & Skan, S. W. (1931). Solutions of the boundary-layer equations. *The London, edinburgh, and dublin philosophical magazine and journal of science*, *12*(80), 865–896. https://doi.org/10.1080/14786443109461870

[4] Hartree, D. R. (1937). On an equation occurring in falkner and skan's approximate treatment of the equations of the boundary layer. *Mathematical proceedings of the cambridge philosophical society* (Vol. 33, pp. 223–239). Cambridge University Press. https://doi.org/10.1017/S0305004100019575

[5] Riley, N., & Weidman, P. D. (1989). Multiple solutions of the Falkner--Skan equation for flow past a stretching boundary. *SIAM journal on applied mathematics*, *49*(5), 1350–1358. https://doi.org/10.1137/0149081

[6] Alam, M. S., Khatun, M. A., Rahman, M. M., & Vajravelu, K. (2016). Effects of variable fluid properties and thermophoresis on unsteady forced convective boundary layer flow along a permeable stretching/shrinking wedge with variable Prandtl and Schmidt numbers. *International journal of mechanical sciences*, *105*, 191–205. https://doi.org/10.1016/j.ijmecsci.2015.11.018

[7] Khan, U., Ahmed, N., Mohyud-Din, S. T., & Bin-Mohsin, B. (2017). Nonlinear radiation effects on MHD flow of nanofluid over a nonlinearly stretching/shrinking wedge. *Neural computing and applications*, *28*, 2041–2050. https://doi.org/10.1007/s00521-016-2187-x

[8] Awaludin, I. S., Ishak, A., & Pop, I. (2018). On the stability of MHD boundary layer flow over a stretching/shrinking wedge. *Scientific reports*, *8*(1), 1–8. https://doi.org/10.1038/s41598-018-31777-9

[9] Waini, I., Ishak, A., & Pop, I. (2021). Melting heat transfer of a hybrid nanofluid flow towards a stagnation point region with second-order slip. *Proceedings of the institution of mechanical engineers, part e: journal of process mechanical engineering*, *235*(2), 405–415. https://doi.org/10.1177/0954408920961213

[10] Waini, I., Ishak, A., & Pop, I. (2019). Hybrid nanofluid flow and heat transfer past a permeable stretching/shrinking surface with a convective boundary condition. *Journal of physics: conference series* (Vol. 1366, p. 12022). IOP Publishing. https://doi.org/10.1088/1742-6596/1366/1/012022

[11] Swain, K., Mebarek-Oudina, F., & Abo-Dahab, S. M. (2022). Influence of MWCNT/Fe_3O_4 hybrid nanoparticles on an exponentially porous shrinking sheet with chemical reaction and slip boundary conditions. *Journal of thermal analysis and calorimetry*, *147*(2), 1561–1570. https://doi.org/10.1007/s10973-020-10432-4

[12] Dinarvand, S., Yousefi, M., & Chamkha, A. (2022). Numerical simulation of unsteady flow toward a stretching/shrinking sheet in porous medium filled with a hybrid nanofluid. *Journal of applied and computational mechanics*, *8*(1), 11–20. https://doi.org/10.22055/jacm.2019.29407.1595

[13] Lund, L. A., Omar, Z., Khan, I., & Sherif, E.-S. M. (2020). Dual solutions and stability analysis of a hybrid nanofluid over a stretching/shrinking sheet executing MHD flow. *Symmetry*, *12*(2), 276. https://www.mdpi.com/2073-8994/12/2/276

[14] Thumma, T., & Mishra, S. R. (2018). Effect of viscous dissipation and Joule heating on magnetohydrodynamic Jeffery nanofluid flow with and without multi slip boundary conditions. *Journal of nanofluids*, *7*(3), 516–526. https://doi.org/10.1166/jon.2018.1469

[15] Pattnaik, P. K., Bhatti, M. M., Mishra, S. R., Abbas, M. A., & Bég, O. A. (2022). Mixed convective-radiative dissipative magnetized micropolar nanofluid flow over a stretching surface in porous media with double stratification and chemical reaction effects: ADM-Padé computation. *Journal of mathematics*, *2022*(1), 9888379. https://onlinelibrary.wiley.com/doi/abs/10.1155/2022/9888379

[16] Thumma, T., Ahammad, N. A., Swain, K., Animasauan, I. L., & Mishra, S. R. (2022). Increasing effects of Coriolis force on the cupric oxide and silver nanoparticles based nanofluid flow when thermal radiation and heat source/sink are significant. *Waves in random and complex media*, 1–18. https://doi.org/10.1080/17455030.2022.2032471

[17] Khashi'ie, N. S., Arifin, N. M., & Pop, I. (2022). Magnetohydrodynamics (MHD) boundary layer flow of hybrid nanofluid over a moving plate with Joule heating. *Alexandria engineering journal*, *61*(3), 1938–1945. https://doi.org/10.1016/j.aej.2021.07.032

[18] Lund, L. A., Omar, Z., Dero, S., Chu, Y., Khan, I., & others. (2020). Temporal stability analysis of magnetized hybrid nanofluid propagating through an unsteady shrinking sheet: Partial slip conditions. *Computers, materials and continua*, *66*(2), 1963–1975. http://dx.doi.org/10.32604/cmc.2020.011976

[19] Khashi'ie, N. S., Waini, I., Arifin, N. M., & Pop, I. (2021). Unsteady squeezing flow of Cu-Al2O3/water hybrid nanofluid in a horizontal channel with magnetic field. *Scientific reports*, *11*(1), 14128. https://www.nature.com/articles/s41598-021-93644-4

[20] Zainal, N. A., Nazar, R., Naganthran, K., & Pop, I. (2021). Stability analysis of MHD hybrid nanofluid flow over a stretching/shrinking sheet with quadratic velocity. *Alexandria engineering journal*, *60*(1), 915–926. https://www.sciencedirect.com/science/article/pii/S1110016820305391

[21] Waini, I., Ishak, A., & Pop, I. (2020). MHD flow and heat transfer of a hybrid nanofluid past a permeable stretching/shrinking wedge. *Applied mathematics and mechanics*, *41*(3), 507–520. https://doi.org/10.1007/s10483-020-2584-7

[22] Dinarvand, S., Rostami, M. N., & Pop, I. (2019). A novel hybridity model for TiO2-CuO/water hybrid nanofluid flow over a static/moving wedge or corner. *Scientific reports*, *9*(1), 16290. https://www.nature.com/articles/s41598-019-52720-6

[23] Shanmugapriya, M., Sundareswaran, R., & Senthil Kumar, P. (2021). Heat and mass transfer enhancement of MHD hybrid nanofluid flow in the presence of activation energy. *International journal of chemical engineering*, *2021*(1), 9473226. https://onlinelibrary.wiley.com/doi/abs/10.1155/2021/9473226

[24] Waini, I., Ishak, A., & Pop, I. (2021). Hybrid nanofluid flow with homogeneous-heterogeneous reactions. *Computers, materials & continua*, *68*(3), 3255–3269. https://cdn.techscience.cn/ueditor/files/cmc/TSP-CMC-68-3/TSP_CMC_17643/TSP_CMC_17643.pdf

[25] Khashi'ie, N. S., Arifin, N. M., Hafidzuddin, E. H., & Wahi, N. (2019). Thermally stratified flow of Cu-Al2O3/water hybrid nanofluid past a permeable stretching/shrinking circular cylinder. *Journal of advanced research in fluid mechanics and thermal sciences*, *63*(1), 154–163. http://semarakilmu.com

[26] Mishra, P., Acharya, M. R., & Panda, S. (2021). Mixed convection MHD nanofluid flow over a wedge with temperature-dependent heat source. *Pramana*, *95*, 1–12. https://doi.org/10.1007/s12043-021-02087-z

[27] Anuar, N. S., Bachok, N., & Pop, I. (2020). Cu-Al2O3/water hybrid nanofluid stagnation point flow past MHD stretching/shrinking sheet in presence of homogeneous-heterogeneous and convective boundary conditions. *Mathematics*, *8*(8), 1237. https://www.mdpi.com/2227-7390/8/8/1237

[28] Anuar, N. S., Bachok, N., Arifin, N. M., & Rosali, H. (2021). Analysis of Al2O3-Cu nanofluid flow behaviour over a permeable moving wedge with convective surface boundary conditions. *Journal of king saud university-science*, *33*(3), 101370. https://www.sciencedirect.com/science/article/pii/S1018364721000318

[29] Gherasim, I., Roy, G., Nguyen, C. T., & Vo-Ngoc, D. (2009). Experimental investigation of nanofluids in confined laminar radial flows. *International journal of thermal sciences*, *48*(8), 1486–1493. https://doi.org/10.1016/j.ijthermalsci.2009.01.008

[30] Mintsa, H. A., Roy, G., Nguyen, C. T., & Doucet, D. (2009). New temperature dependent thermal conductivity data for water-based nanofluids. *International journal of thermal sciences*, *48*(2), 363–371. https://doi.org/10.1016/j.ijthermalsci.2008.03.009

[31] Ahmad, S., Ali, K., Rizwan, M., & Ashraf, M. (2021). Heat and mass transfer attributes of copper–aluminum oxide hybrid nanoparticles flow through a porous medium. *Case studies in thermal engineering*, *25*, 100932. https://www.sciencedirect.com/science/article/pii/S2214157X21000952

[32] Wang, C. Y. (2008). Stagnation flow towards a shrinking sheet. *International journal of non-linear mechanics*, *43*(5), 377–382. https://doi.org/10.1016/j.ijnonlinmec.2007.12.021

[33] Bachok, N., Ishak, A., Nazar, R., & Senu, N. (2013). Stagnation-point flow over a permeable stretching/shrinking sheet in a copper-water nanofluid. *Boundary value problems*, *2013*, 1–10. https://doi.org/10.1186/1687-2770-2013-39

[34] Yacob, N. A., Ishak, A., & Pop, I. (2011). Falkner–Skan problem for a static or moving wedge in nanofluids. *International Journal of Thermal Sciences*, *50*(2), 133-139. https://doi.org/10.1016/j.ijthermalsci.2010.10.008